Journal of Nuclear Materials 385 (2009) 250–257

Contents lists available at ScienceDirect

Journal of Nuclear Materials

journal homepage: www.elsevier.com/locate/jnucmat

Fracture toughness assessment of ferritic–martensitic steel in liquid lead–bismuth eutectic

J. Van den Bosch [a,*], G. Coen [b], A. Almazouzi [a], J. Degrieck [b]

[a] SCK•CEN (Belgian Nuclear Research Centre), Boeretang 200, B-2400 Mol, Belgium
[b] Laboratory for Construction and Production, Ghent University, St. Pietersnieuwstraat 41, B-9000 Ghent, Belgium

ARTICLE INFO

PACS:
61.25.Mv
61.82.Bg
62.20.Mk
68.03.Cd
68.08.−p

ABSTRACT

The presence of micro-cracks at the surface of a ferritic–martensitic steel is known to favour its embrittlement by liquid metals and thus decrease the mechanical properties of the structural materials. Unfortunately, conventional fracture mechanics methods cannot be applied to tests in liquid metal environment due to the opaque and conducting nature of the LBE. Therefore new methods based on the normalization technique for assessment of plain strain fracture toughness in LBE were examined. This paper discusses the assessment of the plain strain fracture toughness of T91 steel in liquid lead bismuth environment at 473 K, tested at a displacement rate of 0.25 mm min^{-1} and makes the comparison with results obtained in air at the same temperature and displacement rate. Although there is a decrease of the fracture toughness by 20–30% when tested in LBE, the toughness of the T91 steel remains sufficient under the tested conditions.

1. Introduction

Liquid lead and lead bismuth eutectic have been selected as working fluids for advanced nuclear applications such as GEN IV, ADS [1,2]. The accelerator driven system (ADS) MYRRHA at the Belgian Nuclear Research Centre, SCK•CEN is designed to have liquid lead bismuth eutectic (LBE) as spallation target material as well as for primary coolant [3].

Although the risk of embrittlement of materials exposed to liquid metals has been recognized for many years, its prediction still remains problematic due to the limited knowledge of the mechanisms involved in the phenomenon. Generally, when solid metals are exposed to liquid metals and stress is applied, they may undergo abrupt brittle failure known as liquid metal embrittlement (LME). It is characterized by a premature brittle failure of an otherwise ductile material when placed in contact with specific liquid metal for the material under stress. LME is of prime interest because of the risk of damage wherever the handling of liquid metals is required. The phenomenon depends on many parameters (intensive and extensive) like metallurgical state, surface state, composition, solubility, temperature, strain rate, stress, etc. [4–6].

For the couple T91–LBE, tensile tests have not given a clear view of the embrittling behaviour of the LBE environment. It was shown by several systematic studies that embrittlement does not always occur under the same conditions [7–9]. The lack of reproducibility of tensile tests performed in LBE was attributed to the absence of wetting. To overcome this problem, relatively exotic methods such as PVD deposition of LBE after ion sputtering or chemical fluxing were used to achieve wetting [10].

However, a distinct LME effect was found without the application of wetting enhancing techniques on notched samples or samples having micro-cracks at the surface in several studies [7,8,11]. This underlined the importance of fracture toughness assessment in liquid metal environment. Unfortunately, the standard fracture mechanics approach cannot be applied to tests in liquid metal environment due to the opaque and conducting nature of the LBE. Auger et al. [12] have made an attempt to assess the fracture toughness of T91 in LBE using CCT specimens. This method is based on the visual observation of the advancing crack. The CCT sample geometry is however loaded in plane stress condition and the results are therefore more relevant for thin wall applications such as cladding tubes. Furthermore, the technique could not allow sufficient crack propagation due to shear band flow localization making it very difficult to draw reliable conclusions. Therefore, we have explored other techniques to assess plain strain fracture toughness in liquid metal environment.

This paper will show the feasibility of plain strain fracture toughness assessment of T91 in liquid metal environment based on three different normalization methods. Furthermore, the more reliable normalization method of the three was determined for the selected application and the obtained results in LBE were compared with those obtained in air.

* Corresponding author. Tel.: +32 14 33 31 77; fax: +32 14 32 12 16.
E-mail address: jvdbosch@sckcen.be (J. Van den Bosch).

0022-3115/$ - see front matter © 2008 Elsevier B.V. All rights reserved.
doi:10.1016/j.jnucmat.2008.11.024

2. Materials

The used T91 ferritic–martensitic steel was delivered by Industeel, ArcelorMittal group as hot rolled and heat treated plates with a thickness of 15 mm. The heat treatment consisted of a normalisation treatment at 1323 K for 15 min followed by a water quench to room temperature. The tempering treatment consisted of heating the normalized steel to 1043 K for 45 min followed by air cooling to room temperature. The chemical composition of the used T91 steel is given in Table 1.

Disc-shaped CT specimens (DCT) were machined in the LT direction (see Fig. 1) and precracked in fatigue to a crack length of $a = 1/2W$, where a is the crack length and W is the width of the specimen.

The LBE material was delivered by Hetzel Metalle GmbH, Germany with a composition of 55.2 wt% Bi and 44.8 wt% Pb, 2 mg g^{-1} Cr and less than 1 mg g^{-1} Ni.

3. Method

Normalization methods were developed to allow fracture toughness assessment in aggressive environments where conventional methods cannot or hardly be applied. These methods are based on calculating the J–R curve, using only the force and displacement data recorded during the test and the initial and final crack length of the tested specimen.

Five reference tests were carried out in air. The DCT specimens were tested at a temperature of 473 K and a displacement rate of 0.25 mm min^{-1}. The crack growth during the reference tests was measured by the unloading compliance method and the potential drop method. To examine the applicability of the three normalisation methods to the used sample geometry and material type, J–R curves for these reference tests in air were also calculated by applying the three normalization methods. This approach showed the uncertainty of the obtained indirect J–R curves compared to the J–R curves obtained by online monitoring of the growing crack.

For tests in LBE, a reservoir was mounted onto the load line. Once the material had reached 473 K, the LBE was poured into the reservoir submerging the DCT specimen. The LBE reservoir was mechanically tapped on, to remove possible air bubbles. No chemical fluxing was used to promote wetting. Results by Long and Dai [13] have shown that no chemical fluxing is needed to achieve reproducible results on liquid metal embrittlement of precracked specimens due to the presence of the fatigue crack at the surface.

The test was started after the temperature settled at 473 ± 2 K for 20 min following the recommendations of standard ASTM E 1820.

For tests in LBE, no clip gauge could be used. Instead of the clip gauge data, the displacement data recorded by the test bench (stroke) had to be used. This decreases the accuracy of the J–R curve because the compliance of the entire loading line is comprised in the stroke signal in contrast with the CMOD signal which only comprises the compliance of the specimen due to the local measurement. However, this decrease in accuracy can be limited to a minimum by the application of a compliance correction to the displacement data. The compliance correction is in fact nothing more than a mathematical correction which makes every load–displacement curve of each reference test based on the CMOD signal coincides with the load–displacement curve of the same reference test based on the stroke signal.

Since the reference tests in air were performed using a clip gauge and the tests in LBE were performed on the same test bench at the same temperature, the difference between the displacement signal of the clip gauge (CMOD) and this of the test bench actuator (stroke) could be corrected for the tests in LBE without having

Table 1
Composition of the ferritic–martensitic steel T91 (wt%).

C	N	Al	Si	P	S	Ti	V	Cr	Mn	Ni	Cu	As	Nb	Mo	Sn	W
0.10	0.0442	0.015	0.22	0.021	0.0004	0.003	0.21	8.99	0.38	0.11	0.06	0.008	0.06	0.89	0.004	0.01

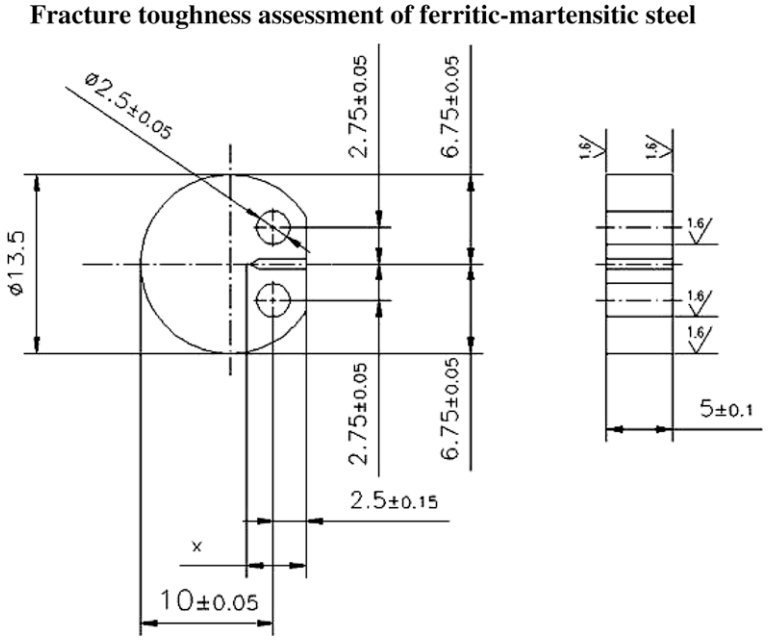

Fig. 1. Schematic representation of the disc-shaped in tension (DCT) specimen; dimensions in mm.

actual CMOD data. This assumes the compliance of the test rig is not altered by attaching the small LBE reservoir to the load line.

To calculate the compliance correction, a linear fit was made of the force as a function of the difference between the stroke and crack mouth opening displacement (CMOD) for each of the reference tests in their elastic area. The average of the linear factors and terms over the five reference tests were taken. This results in the following compliance correction model applicable only to the used test set-up at 473 K

$$F(N) = 9.893\ \mathrm{Nmm^{-1}} \times (\mathrm{Stroke} - \mathrm{CMOD}) - 0.138\mathrm{N} \quad (1)$$

Force–displacement curves of both the tests performed in air and in LBE are shown in Fig. 2. Note that the slope of the elastic part of these curves before compliance correction is not the same since the upper curves are based on CMOD data and the lower curves are based on stroke data.

The normalization methods applied in this study are briefly explained in the following paragraphs.

3.1. Chaouadi method

The Chaouadi method [14] is based on the observation that the normalized crack extension varies as the square of the normalized energy.

$$\frac{\Delta a}{\Delta a_f} \approx \left(\frac{E - E_i}{E_f - E_i}\right)^2 \quad (2)$$

where E is the absorbed energy, i.e. the area under the load–displacement curve, E_i is the crack initiation energy and E_f and Δa_f are the total energy and associated crack extension of the tested specimen. For the calculation of E_i, the author made the common assumption that crack initiation occurs at a load equal to the average of the general yield and maximum load [14]. This assumption was based on the experimental observation that ductile crack initiation occurs somewhere between the general yield load and the maximum load. Furthermore, it is supported by a large amount of data including Charpy impact test data and crack initiation detection measurements.

After the calculation of E and Δa for each data point of the force–displacement data, the value of the J-integral is calculated using the equation for J of disc-shaped compact tension specimens as stated in ASTM E 1820. When using non standard specimen geometries the following equation for J could be applied instead of this of ASTM E 1820:

$$J = J_i + J_t\sqrt{\Delta a} \quad (3)$$

where J_i is the ductile crack initiation toughness and J_t the tearing resistance toughness [14].

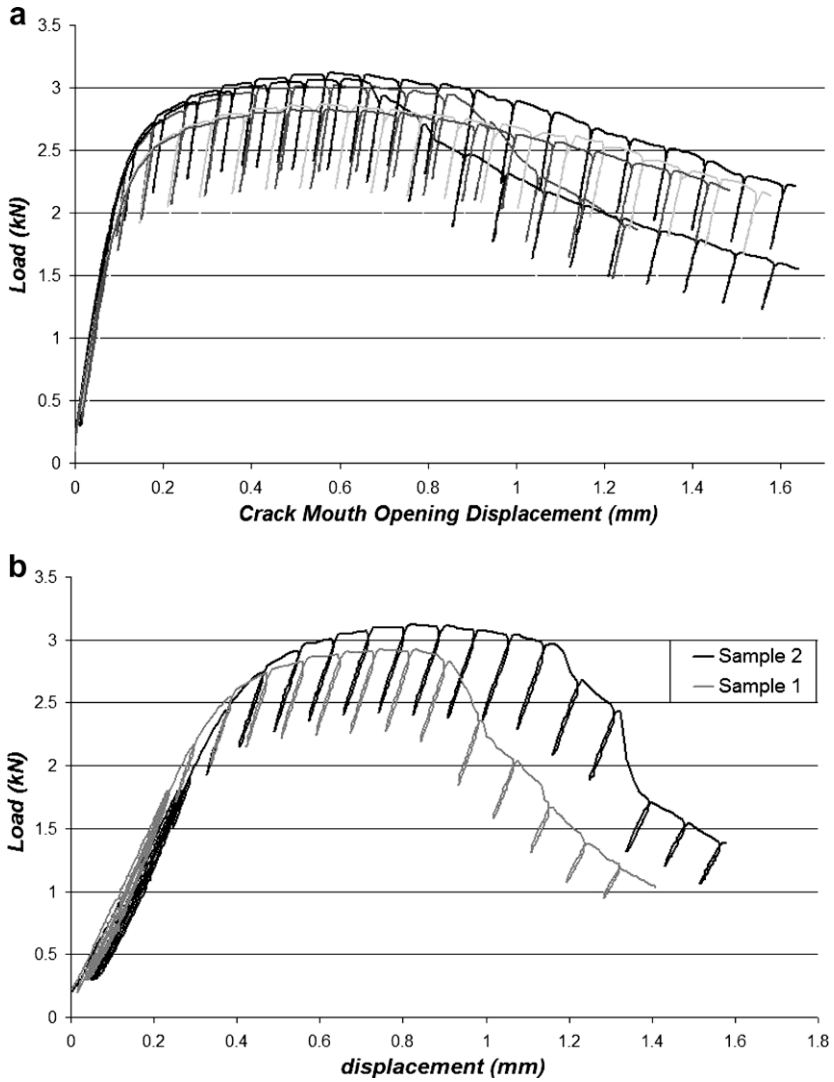

Fig. 2. (a) Load–crack mouth opening displacement curves of tests in air at 473 K and 0.25 mm min^{-1}; load–stoke curves of tests in LBE at 473 K and 0.25 mm min^{-1}.

Empirical fits of J–Δa curves very often show a power law kind of curve, not linear. The exponent that is derived is often close to 0.5, which is the square root dependence. In this work, we used the equation for the J-integral of DCT specimens as stated in ASTM E 1820.

3.2. Donoso et al. method

The Donoso method [15] generates the J–R curve in closed analytical form, using the Common and Concise Formats, developed by Donoso et al. [15]. In this method, a crack growth law for plastic displacement is proposed, that relates the change in crack length, Δa, and the normalized plastic displacement:

$$\frac{\Delta a}{W} = l_0\left(\frac{v_{pl}}{W}\right)^{l_1} \tag{4}$$

with W the width of the specimen. Using this crack growth law and the final values of the force, displacement and crack size, the value of l_0 is calculated for l_1 ranging from 1.5 to 2.5.

Starting from a tentative list of v_{pl}, the plastic displacement, the values of the force P are calculated using the Common Format Equation (CFE) for each of the values of v_{pl} in the list:

$$P = \Omega^* \sigma^* BCW\left(\frac{b_0}{W} - l_0\left(\frac{v_{pl}}{W}\right)^{l_1}\right)^m \left(\frac{v_{pl}}{W}\right)^{\frac{1}{n}} \tag{5}$$

B = thickness of the specimen; Ω^* = the constraint factor; σ^* = coefficient of the plasticity hardening function, it can be obtained from a stress–strain curve as described in [16]; m = the exponent of geometry function in plasticity and equals 2.2360 for compact specimens [16]; C = the coefficient of the geometry function of plasticity and equals 1.553 [16]. C is considered as a constant, although C may be dependent on m and on the ligament size b/W for compact specimens; n = hardening exponent in the Ramberg–Osgood equation [16]; b_0 = original remaining ligament.

Next, the value of l_1, which gives the best match between the experimental curve and the model P–v curve is selected. Fig. 3 shows an example of this fit, the selected values for this test are $l_0 = 12.36$ and $l_1 = 2.50$.

Once the values for l_0 and l_1 for the test are known, Δa is calculated for each of the values in the v_{pl} list using the crack growth law with the selected values of l_0 and l_1.

Finally the elastic and plastic component of the J-integral are calculated using the equations for J_e and J_{pl} [15].

3.3. Normalization data reduction (NDR) method

The normalization data reduction method, described in Annex A15 of the ASTM E 1820 standard was the third normalization technique applied to the test results.

4. Results and discussion

To validate the normalization methods, a comparison was made between the J–R curves of the normalization methods, the unloading compliance and potential drop method for one of the reference tests, performed in air. These curves are depicted in Fig. 4. The average of the values of the J–R curves produced by the conventional online crack advance measuring techniques, being unloading compliance and potential drop method was calculated. This average ±15% is also shown in Fig. 4, because this is the expected scatter between different analysis methods for fracture toughness tests as accepted by ASTM E 1820.

There is a very good similarity between the test results and the results from the normalization methods. The different curves nicely illustrate the scatter of ±15% in fracture toughness tests. The curve constructed by the Chaouadi method is in very good agreement with the unloading compliance results. The curve resulting from the Donoso and Landes method, smoothes near the end. The same descent is visible in Fig. 3 and originates from a final crack size which is slightly larger than the maximum crack size permitted by ASTM E 1820 for the application of the NDR method.

To validate the compliance correction, a comparison was made between the results of the normalization methods applied to the CMOD data, the stroke data and the model applied to the stroke data from the reference tests. As an example, the results of the Donoso and Landes method is given in Fig. 5. Without compliance correction, the Donoso and Landes curve constructed with stroke data, lies clearly above the curve constructed with CMOD data +15%. The curve resulting form corrected data, lies within the normal scatter.

After the validation of the normalization methods, the three different methods were applied to tests performed at the same temperature and applying the same speed, but executed in LBE. Two tests showed clear signs of LME. The force–displacement curves, shown in Fig. 2, show sudden drops in force with increasing displacement.

The embrittlement was also clearly visible in the J–R curves. Fig. 6 shows the J–R curves calculated by the three normalization methods for both embrittled specimens, tested in LBE.

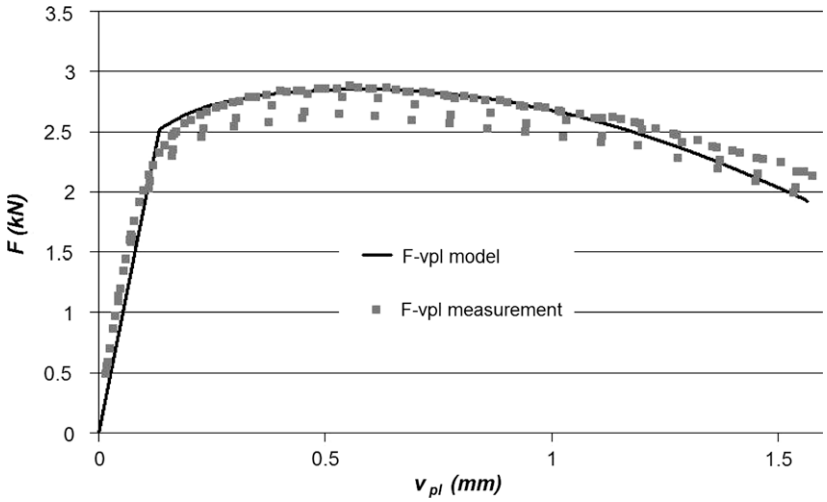

Fig. 3. Comparison of measured force–displacement curve and force–displacement curve according to the common format equation (CFE) with the fitted l_0 and l_1 values.

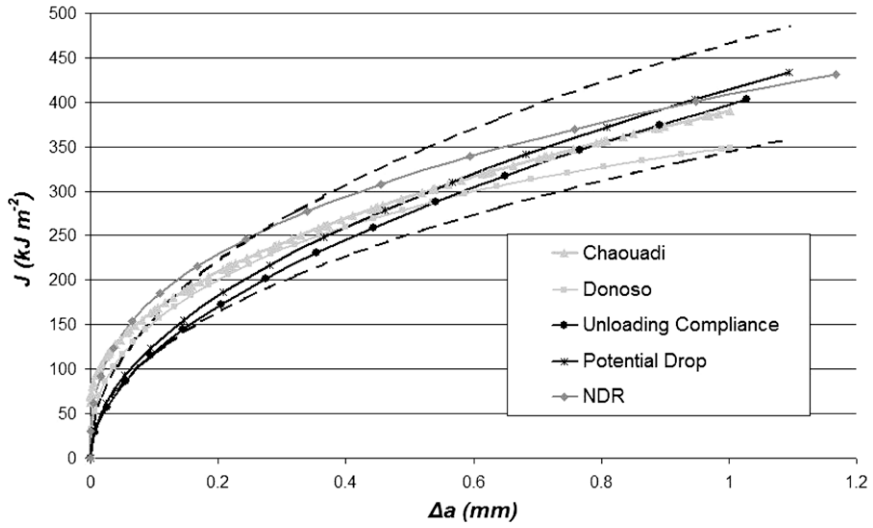

Fig. 4. *J–R* curves of different test and normalization methods for reference test in air at 473 K and 0.25 mm min^{-1}; experimental uncertainty of ±15% indicated by dashed lines.

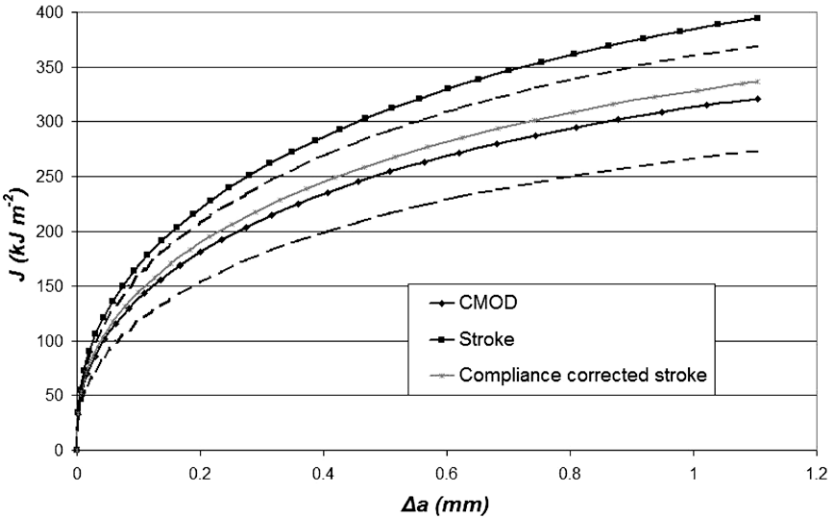

Fig. 5. *J–R* curve of Donoso method applied to CMOD; stroke and compliance correction model data; experimental uncertainty of ±15% indicated by dashed lines.

In Fig. 7, the average *J–R* curve of a reference test is compared to the average *J–R* curve of the test showing the most embrittlement in LBE. These average curves were constructed by calculating the average of all applied analysis methods for the same test. It is clear that the *J*-integral values of the embrittled sample are lower than the average of the reference curves minus the 15% scatter. The *J–R* curves clearly show the embrittlement of the specimen by LBE.

SEM investigation of the crack surfaces of both specimens tested in LBE showed clear signs of embrittlement. This indicates there was wetting between the liquid lead bismuth and the T91 steel at the advancing crack tip.

The surface of sample 1 exhibits mixed ductile and brittle fracture characteristics across the entire fracture surface. A detail of the fracture surface is shown in Fig. 8. It seems that individual grains were fractured in cleavage mode whereas other grains fractured in ductile mode. Several grains which cracked in cleavage mode are indicated by arrows in Fig. 8. It is however clear that many more grains which cracked in cleavage can be found in the picture. An area which shows a relatively high fraction of dimples has been circled in Fig. 8. When examining this area more in detail however, one can still find small regions which cracked in cleavage fracture mode. This difference in fracture mode is probably due to the orientation of the grains in respect to the crack surface plane and the related tendency to cleavage in these orientations.

The surface of sample 2 exhibits a few local fully brittle fracture sites combined with mixed ductile and brittle fracture characteristics across the majority of the sample's fracture surface. Picture A in Fig. 9 shows a fully brittle crack initiation site which is located at the notch of the side groove on the side of the sample. This indicates that the crack advancement was not solely initiated at the precrack which is the case for fracture toughness tests in air. Picture B in Fig. 9 shows a detail of the middle of the sample's fracture surface. The upper left in Fig. 9B is a grain which fully cracked in cleavage whereas in the lower left of the picture, the fracture surface reveals very similar characteristics to the fracture type shown in Fig. 8.

As a single value to characterize the fracture toughness, the J_q value was calculated for each of the normalization methods

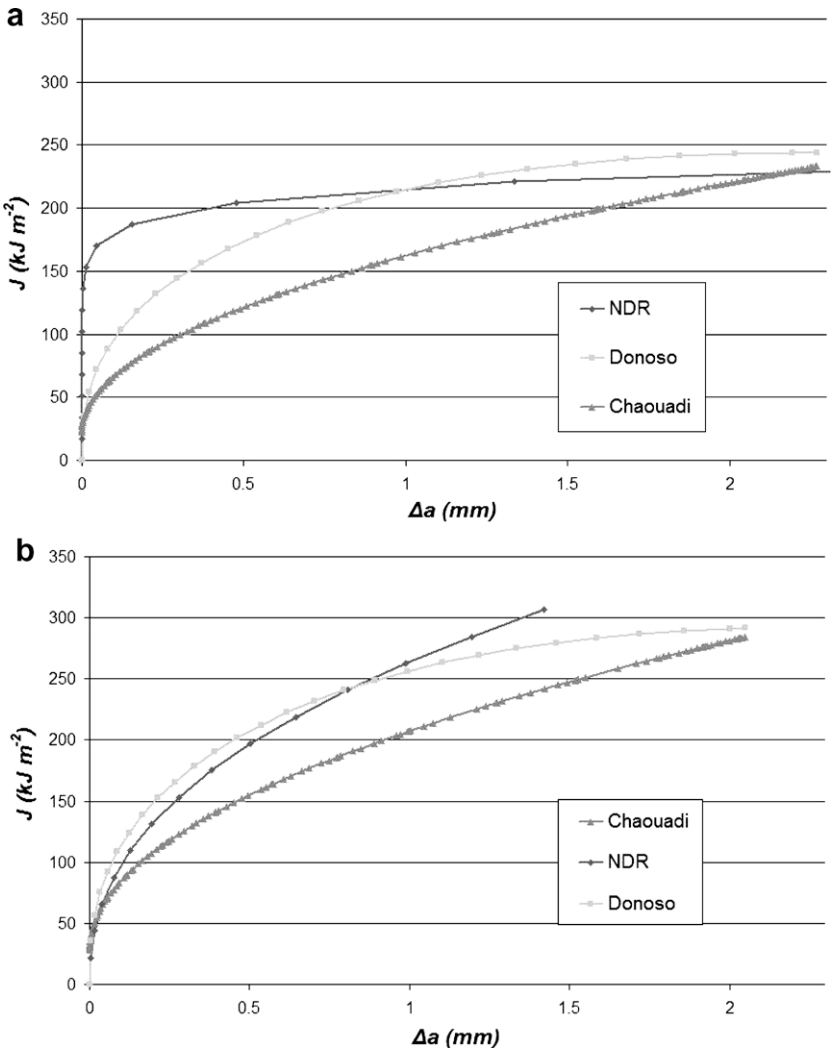

Fig. 6. *J–R* curves of normalization methods applied to test data in LBE at 473 K and 0.25 mm min^{-1} of (a) sample 1 and (b) sample 2.

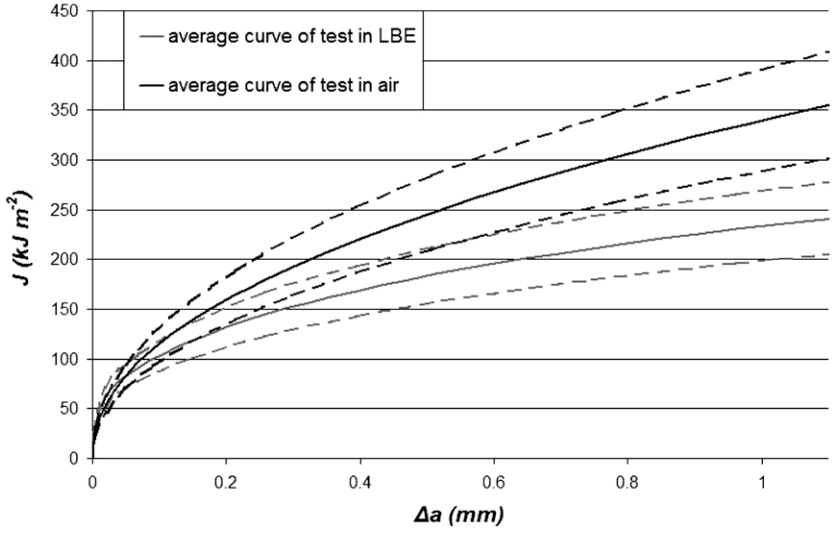

Fig. 7. Comparison of *J–R* curves in air and LBE; experimental uncertainty of ±15% indicated by dashed lines.

according to ASTM E 1820. The J_q value calculated is not valid as J_{Ic} value, which characterizes the toughness of a material near the onset of crack extension from a pre-existing fatigue crack, because the requirements are not met.

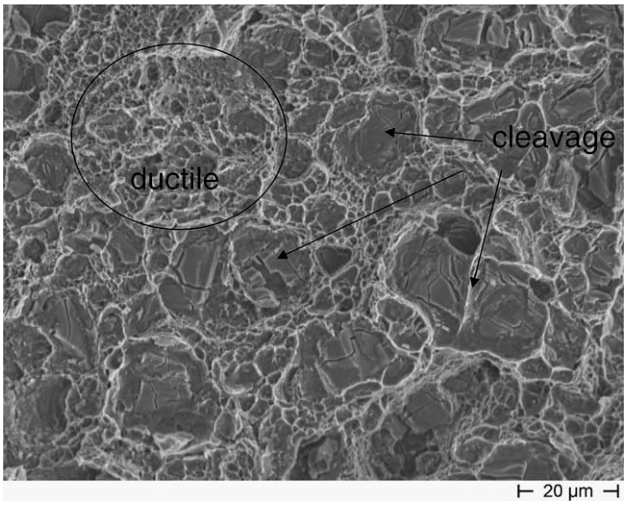

Fig. 8. SEM of the mixed ductile–brittle fracture surface of sample 1. Several grains which cracked in cleavage mode are indicated by arrows. Note that many more cleaved grains can be seen in the picture. A region with a relatively high fraction of dimples was circled. More detailed investigation of this area also reveals small areas cracked in cleavage mode.

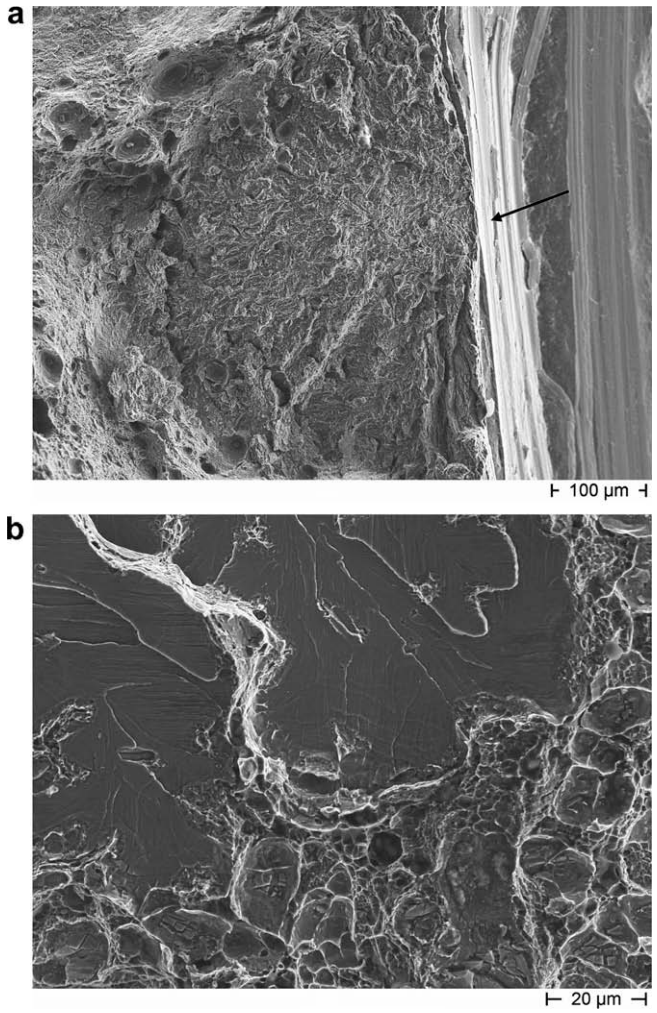

Fig. 9. SEM of fracture surface of sample 2: (a) pseudo-cleavage fracture initiation site in the notch of the side groove on the side of the sample; (b) detail of local brittle fractured grain surrounded by mixed ductile–brittle fracture areas in the middle of the sample's fracture surface.

Table 2
Comparison of Jq values for tests in air and in LBE (kJ m^{-2}).

Average of reference tests (air)	Average of normalization methods for sample 1 (LBE)	Average of normalization methods for sample 2 (LBE)
223.0	138.5	174.8

$$B > 25J_q/\sigma_y$$
$$b_o > 25J_q/\sigma_y$$

In Table 2, a comparison is made between the average value of J_q resulting from the test data of the reference tests, which serves as reference value, and an average J_q value resulting from normalization methods applied to the two tests in LBE. Although the values are not valid as J_{Ic} values, they give a clear indication of the decrease of the plain strain fracture toughness when tested in LBE.

5. Conclusions

Based on the results obtained in this work, the following conclusions can be stated:

1. Normalization methods can be used for tests performed in liquid metals to construct J–R curves using limited input like force–displacement test data, and initial and final crack size.
2. All three normalization methods are applicable and there is no single method which always gives the best results. Therefore, we have applied all three methods and calculated the average. The method by Chaouadi is the easiest to apply and gives very good results for standard geometries. No problems were reported using the NDR method, except in cases where the smoothness of the curve was not ideal. The method by Donoso and Landes is widely applicable and shows good results, the only disadvantage lies in the fact that it requires the fine-tuning of many parameters.
3. When a clip gauge cannot be used, its recommended to apply a compliance correction.
4. Based on the obtained results, the plain strain fracture toughness of T91 steel at 473 K and at a displacement rate of 0.25 mm min^{-1} is by decreased by 20–30% in LBE compared to the fracture toughness in air.

Acknowledgements

This work was partly supported by the European project IP-EUROTRANS-DEMETRA (FI6W-CT-2004-516520).

References

[1] C. Rubbia, J.A. Rubio, S. Buono, F. Carmianti, N. Fietier, J. Galvez, C. Geles, Y. Kadi, R. Klapish, P. Mandrillioni, J.P. Revol, C. Roche, CERN Report AT/95-44 (ET), 1995.
[2] H.U. Knebel, X. Cheng, C.H. Lefhalm, G. Müller, G. Schumacher, J. Konys, H. Glasbrenner, Nucl. Eng. Des. 202 (2000) 279.
[3] H. A Abderrahim, P. Kupschus, E. Malambu, Ph. Benoit, K. Van Tichelen, B. Arien, F. Vermeersch, P. D'hondt, Y. Jongen, S. Ternier, D. Vandeplassche, Nucl. Instrum. and Meth. A 463 (2001) 487.
[4] W. Rostoker, J.M. McCoughy, M. Markus, Embrittlement by Liquid Metals, Reinhold, Chapman and Hall, New York, London, UK, 1960.
[5] M.H. Kamdar, Prog. Mater. Sci. 15–4 (1973) 289.
[6] B. Joseph, M. Picat, F. Barbier, Eur. Phys. J. AP 5 (1999) 19.
[7] J. Van den Bosch, D. Sapundjiev, A. Almazouzi, J. Nucl. Mater. 356 (2006) 237.
[8] Y. Dai, B. Long, F. Groeschel, J. Nucl. Mater. 356 (2006) 222.
[9] F. Di Gabriele, A. Doubková, A. Hojná, J. Nucl. Mater. 376 (3) (2008) 307.

[10] T. Auger, G. Lorang, S. Guérin, J.-L. Pastol, D. Gorse, J. Nucl. Mater. 335 (2004) 227.
[11] J. Van den Bosch, R.W. Bosch, D. Sapundjiev, A. Almazouzi, J. Nucl Mater. 376 (3) (2008) 322.
[12] T. Auger, Z. Hamouche, L. Medina-Almazan, D. Gorse, J. Nucl. Mater. 377 (1) (2008) 253.
[13] B. Long, Y. Dai, J. Nucl. Mater. 376 (3) (2008) 341.
[14] R. Chaouadi, Journal of Testing and Evaluation 32 (6) (2004) 469.
[15] J.R. Donoso, J. Zahr, J.D. Landes, J. ASTM Int. 2 (3) (2005) 1.
[16] J.R. Donoso, J.D. Landes, Eng. Fr. Mech. 47 (1994) 619.